

Simulation of Floating Bodies in Waves and Mooring in a 3D Numerical Wave Tank Using REEF3D



Tobias Martin, Hans Bihs, Arun Kamath and Øivind Asgeir Arntsen

Abstract Mooring systems ensure the safety of structures near the shore like floating breakwaters and aquaculture cages by keeping them in position. Their design has to either provide enough flexibility to allow large displacements or enough strength to withstand the hydrodynamic loads while restraining the structural motion. The accurate determination of the motion of the moored-floating structure and the resulting tension forces in the cables is, therefore, of high significance to produce a safe and economical design. At the same time, the dynamics of the cables can be neglected in the early design process due to their minor contribution to the forces acting on the structure. Hence, an analytical solution for the cables can be found, which provides a fast solution to the problem. The mooring model is implemented in the open-source CFD model REEF3D. The solver has been widely used to study various problems in the field of wave hydrodynamics. It solves the incompressible Reynolds-averaged Navier–Stokes equations for two-phase flows using a finite-difference method and a level set method to model the free surface between water and air. Floating structures are represented by an additional level set function. Its motion is calculated from the Newton and Euler equations in 6DOF and in a non-inertial coordinate system. The fluid–structure interaction is solved explicitly using an immersed boundary method based on the ghost cell method. The application shows the accuracy of the solver and effects of mooring on the motion of a floating structure.

Keywords CFD · REEF3D · Mooring · Fluid–structure interaction

T. Martin (✉) · H. Bihs · A. Kamath · Ø. A. Arntsen
Norwegian University of Science and Technology, 7491 Trondheim, Norway
e-mail: tobias.martin@ntnu.no

A. Kamath
e-mail: arun.kamath@ntnu.no

© Springer Nature Singapore Pte Ltd. 2019
K. Murali et al. (eds.), *Proceedings of the Fourth International Conference in Ocean Engineering (ICOE2018)*, Lecture Notes in Civil Engineering 22,
https://doi.org/10.1007/978-981-13-3119-0_44

1 Introduction

Coupled fluid–structure interaction plays a major role in the fields of coastal and ocean engineering. Most applications require the solution of a two-phase problem as well as an accurate determination of rigid body dynamics. Some examples are floating breakwater, aquaculture cages or ship motion prediction. As a first attempt, fluid–structure interaction problems based on the Navier–Stokes equations have been calculated with Arbitrary Lagrangian–Eulerian methods [18]. In this approach, the interface between solid and fluid is tied to the numerical mesh for which reason the mesh needs to be adjusted dynamically. The re-meshing procedure can have a detrimental effect on the numerical accuracy and stability, especially for more arbitrary solid body movements. A way to avoid constant re-meshing is the usage of dynamic overset grids. The method consists of a Eulerian mesh for the fluid and a overset mesh which follows the movement of the solid and overlaps with the base mesh. A stable scheme for establishing the connections between the overset mesh points and the underlying grid points in the overlapping region has to be introduced (see, e.g. [7]). As an alternative, a direct forcing immersed boundary method was developed for describing the fluid–structure interaction [26]. This immersed boundary method requires just one Eulerian grid, and the interaction is incorporated by an additional forcing term in the Navier–Stokes equations. Special attention was also given to the field extension method [24], which accounts for solid cells becoming fluid cells and vice versa. With the field extension, unphysical values for the pressure and the velocities are avoided. More recently, [6] presented a level set-based two-phase flow solver for the simulation of floating structures. In this work, an extension of the local directional immersed boundary method [2] using the field extension method is presented. The geometry of the solid is described by a level set function. Hence, forces and moments can be calculated without explicitly defining the intersections between the surface mesh and the grid of the flow domain. Like other immersed boundary methods, the solid body is immersed into the fluid and re-meshing or overset grids are avoided. The presented results are all obtained with a weakly coupled scheme. In combination with the robust two-phase flow solver REEF3D [4], this results in a stable fluid–structure interaction model. If the motion of the floating structure is large, mooring dynamics can have a significant impact on the response of the structure. The general solution for the dynamics of mooring systems has to be found numerically due to the underlying nonlinear system of equations. Several discretisation methods have been developed, like the finite differences [13] and finite element-based methods [1] or the lumped mass method [12]. A general overview of the methods can be found in [9]. For structures with small responses in mild environmental conditions, a quasi-static mooring model is suitable. By neglecting the dynamic effects of the mooring system, dependencies of mass, damping and fluid acceleration on the system are omitted. The mooring line shape and tension can then be found analytically as shown by [10]. It has the advantage of computational efficiency and simplicity of implementation. Therefore, the analytical approach is taken into account in this paper as a starting point for more advanced models in further research. In Sect. 2,

the CFD model REEF3D is shortly described. Afterwards, details about the implemented 6DOF algorithm and mooring model are given in Sects. 2.1 and 2.2. The application of the solver is presented in Sect. 3. Final remarks and prospects for further developments can be found in Sect. 4.

2 Numerical Model

The basic equations of the numerical model arise from the conservation law of mass and momentum for incompressible fluids. Using tensor notation, the resulting equations read for a whole-domain formulation

$$\frac{\partial u_i}{\partial x_i} = 0, \quad (1)$$

$$\frac{\partial u_i}{\partial t} + u_j \frac{\partial u_i}{\partial x_j} = -\frac{1}{\rho} \frac{\partial p}{\partial x_i} + \frac{\partial}{\partial x_j} \left(\nu \cdot \left(\frac{\partial u_i}{\partial x_j} + \frac{\partial u_j}{\partial x_i} \right) \right) + g_i, \quad (2)$$

with u_i the velocity components, ρ the fluid density, p the pressure, ν the kinematic viscosity and \mathbf{g} the gravity acceleration vector. Here, the Reynolds-averaged Navier–Stokes (RANS) equations are solved by replacing the fluid properties with time-averaged values and add turbulent viscosity to ν . The additional viscosity is calculated with a modified k - ω model as given in [4].

The spatial domain is discretised by a finite-difference method (FDM) on a Cartesian grid. System (1), (2) is solved on a staggered grid to avoid decoupling of pressure and velocity. Convection terms are evaluated in a non-conservative form because the violation of the mass conservation during an explicit solution procedure might cause numerical instabilities in a conservative formulation [21]. For this purpose, the fifth-order accurate weighted essentially non-oscillatory (WENO) scheme of [15] adapted to non-conservative terms by [27] is applied. The discretised system is solved using Chorin’s projection method for incompressible flows [8]. The pressure is calculated from a Poisson equation and by applying the fully parallelised BiCGStab algorithm [23]. For progressing in time, the third-order accurate Total Variation Diminishing (TVD) Runge–Kutta scheme [20] is employed. Adaptive time stepping controls the time stepping according to the required CFL condition.

The location of the free water surface is represented implicitly by the zero level set of a smooth signed distance function $\Phi(\mathbf{x}, t)$ which is defined as the closest distance to the interface [16]. Its motion can be described by the advection equation

$$\frac{\partial \Phi}{\partial t} + u_j \frac{\partial \Phi}{\partial x_j} = 0. \quad (3)$$

The convection term in (3) is discretised by the fifth-order accurate Hamilton–Jacobi WENO method of [14]. In order to conserve the signed distance property,

the level set function is reinitialised after each time step. Here, the PDE-based reinitialisation equation of [21] is taken into account. The material properties of the two phases are finally determined for the whole domain in accordance with the continuum surface force model of [5] (see [4] for details).

2.1 6DOF Algorithm

The geometry of the rigid body is described by a primitive triangular surface mesh neglecting connectivity. For this purpose, the intersections of the surface mesh with the underlying Cartesian grid are determined with the ray-tracing algorithm of [25]. It efficiently provides inside–outside information and, for each grid point, the shortest distance along the coordinate axis to the body describing triangles. Afterwards, the mentioned reinitialisation algorithm of [17] is applied to obtain signed distance properties for a level set function in the vicinity of the solid body. This has the advantage that the intersections of the surface mesh with the underlying grid do not have to be calculated explicitly. The obtained level set function can be used for calculating the six force and moment components of the fluid on the body as given by [3].

Any point relating to a rigid body can be described by the location of the centre of gravity and orientation of the body in the inertial coordinate system. Here, the orientation is described by Euler angles which results in the position vector

$$\mathbf{x} = (x_1, x_2, x_3, x_4, x_5, x_6)^T, \quad (4)$$

where the first three components are the coordinates of the centre of gravity and the last three components are the Euler angles ϕ , θ and ψ . The calculation of the motion of a body in the inertial system would include several time derivatives of moments which can be avoided by applying a coordinate transformation to the Euler equations. The rotation components in the principal coordinate system of the body reads then

$$\boldsymbol{\xi} = (\xi_1, \xi_2, \xi_3)^T. \quad (5)$$

In this paper, it is assumed that the principal axes of the body are known. Thus, the inertia tensor reduces to the three principal moments of inertia which yields

$$\mathbf{I} = \begin{bmatrix} I_x & 0 & 0 \\ 0 & I_y & 0 \\ 0 & 0 & I_z \end{bmatrix} = \begin{bmatrix} mr_x^2 & 0 & 0 \\ 0 & mr_y^2 & 0 \\ 0 & 0 & mr_z^2 \end{bmatrix}, \quad (6)$$

with m the mass of the body and r_x , r_y and r_z the distances of a point from the centre of gravity along the x -, y - and z -direction. Since the fluid flow is calculated in the inertial system, the acting moments in this system \mathbf{M}_x have to be transformed to the non-inertial system by applying the transformation [11]

$$\mathbf{M}_{\xi} = (M_{1,\xi}, M_{2,\xi}, M_{3,\xi})^T = \mathbf{J}_1^{-1} \cdot \mathbf{M}_x, \quad (7)$$

with \mathbf{M}_{ξ} the moments in the system of the body and \mathbf{J}_1^{-1} the rotation matrix (s stands for sin and c for cos)

$$\mathbf{J}_1 = \begin{bmatrix} cx_6cx_5 & -sx_6cx_4 + cx_6sx_5sx_4 & sx_6sx_4 + cx_6cx_4sx_5 \\ sx_6cx_5 & cx_6cx_4 + sx_4sx_5sx_6 & -cx_6sx_4 + sx_5sx_6cx_4 \\ -sx_5 & cx_5sx_4 & cx_5cx_4 \end{bmatrix}. \quad (8)$$

Hence, the dynamics of the rigid body can be described by the three equations of translational motion

$$\begin{pmatrix} \ddot{x}_1 \\ \ddot{x}_2 \\ \ddot{x}_3 \end{pmatrix} = \frac{1}{m} \cdot \begin{pmatrix} F_{x_1,x} \\ F_{x_2,x} \\ F_{x_3,x} \end{pmatrix}, \quad (9)$$

where F_x are the acting forces in the inertial system and the three Euler equations in the non-inertial system are [11]

$$\begin{aligned} I_x \ddot{\xi}_1 + \dot{\xi}_2 \dot{\xi}_3 \cdot (I_z - I_y) &= M_{1,\xi}, \\ I_y \ddot{\xi}_2 + \dot{\xi}_1 \dot{\xi}_3 \cdot (I_x - I_z) &= M_{2,\xi}, \\ I_z \ddot{\xi}_3 + \dot{\xi}_1 \dot{\xi}_2 \cdot (I_y - I_x) &= M_{3,\xi}. \end{aligned} \quad (10)$$

The position of the body can be calculated analytically by integrating (9) twice. System (10) is solved explicitly with the second-order accurate Adams–Bashforth scheme which reads for a generic variable in the new time step $q^{(n+1)}$

$$\dot{q}^{(n+1)} = \dot{q}^{(n)} + \frac{\Delta t}{2} \cdot (3\ddot{q}^{(n+1)} - \ddot{q}^{(n)}), \quad (11)$$

$$q^{(n+1)} = q^{(n)} + \frac{\Delta t}{2} \cdot (3\dot{q}^{(n+1)} - \dot{q}^{(n)}). \quad (12)$$

The Euler angles in the body system cannot be calculated from the body angular velocities due to missing physical interpretation [11]. Instead, the angular velocities are transformed back using the rotation matrix [11] (s stands for sin, c for cos and t for tan)

$$\mathbf{J}_2 = \begin{bmatrix} 1 & sx_4tx_5 & cx_4 + cx_6tx_5 \\ 0 & cx_4 & -sx_4 \\ 0 & sx_4/cx_5 & cx_4/cx_5 \end{bmatrix}. \quad (13)$$

Afterwards, the necessary Euler angles are calculated from (12) in the inertial frame. It might be noticed that (13) has a singularity at $x_5 = \pm \frac{\pi}{2}$. In practice, this angle does not occur for typical floating structures in ocean engineering.

In this paper, the fluid–structure coupling is arranged in a weak form without sub-iterations. First, acting forces are calculated from the fluid, and the body position is determined as described above. Afterwards, the fluid properties are updated to the new time level using the ghost cell immersed boundary method [2] for incorporating the boundary conditions of the solid. For both the velocities and the pressure, these conditions are calculated from the motion of the body with respect to its centre of gravity [3]. Even though the weak coupling has been reported to lead to numerical stability problems for complex cases (e.g. [6] or [7]), the current implementation shows good numerical stability throughout the range of application. However, pressure oscillations can occur in the vicinity of the solid body because of solid cells turning into fluid cells. The fresh fluid cells lack physical information about velocities from previous time steps. It is solved by implementing the field extension method of [22, 24] adapted to the ghost cell immersed boundary method.

2.2 Mooring Model

The mooring systems considered in this paper consist of a number of cables which are attached to the floating structure at arbitrary points. Their lower ends are anchored at the seabed. In order to avoid high vertical forces on the anchor, a part of the cable lies on the bottom and damps the vertical motion of the structure. An illustration of this configuration can be seen in Fig. 1. The general equations describing the unsteady motion of a cable are nonlinear and have to be solved numerically. For practical purposes, an analytical solution can be found if static conditions and no current forces are assumed. Following the derivation of [10], a catenary equation, describing the shape of a line, arises as

$$z(x, y) = \frac{F_h}{w} \cdot \left(\cosh \left(\frac{w}{F_h} \cdot \sqrt{x^2 + y^2} \right) \right), \tag{14}$$

with F_h the horizontal force, which is constant along the cable, and w the weight per unit length of the cable in water. The tension forces F_t are calculated as

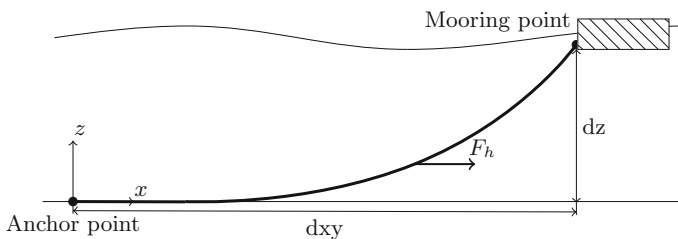


Fig. 1 Definition of a mooring line in two dimensions

$$F_t(z) = F_h + wdz + (z - dz) \cdot (w + \rho gA), \tag{15}$$

where g is the acceleration due to gravity and A is the cross-section area of the cable. The area is assumed to be constant; i.e. elasticity of the material is neglected. In the current algorithm, the effect of the mooring lines on the dynamics of the structure is taken into account explicitly in a weakly coupled manner. For this purpose, the forces of each cable acting on the structure have to be calculated from the known distance dxy from the time-invariant anchor point to the current position of the mooring point. The corresponding equation is written as [10]

$$dxy = \sqrt{dx^2 + dy^2} = l - dz \cdot \sqrt{1 + 2 \cdot \frac{F_h}{wdz}} + \frac{F_h}{w} \cosh^{-1} \left(1 + \frac{wdz}{F_h} \right), \tag{16}$$

which provides a function transcendental in F_h . A solution can be determined using the Newton–Raphson algorithm

$$F_h^{(k+1)} = F_h^{(k)} - \frac{f(F_h^{(k)})}{f'(F_h^{(k)})}, \quad k = 1, 2, \dots \tag{17}$$

Once, a converged solution for F_h has been found, the forces at each mooring point X, Y, Z result from

$$X = F_h \cos \left(\tan^{-1} \left(\frac{dy}{dx} \right) \right), \tag{18}$$

$$Y = F_h \sin \left(\tan^{-1} \left(\frac{dy}{dx} \right) \right), \tag{19}$$

$$Z = F_h dz \cdot \sqrt{1 + \frac{2F_h}{wdz}}, \tag{20}$$

and moments by multiplication with the appropriate distances to the centre of gravity of the body.

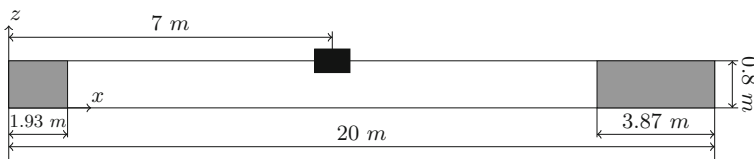


Fig. 2 Setup for the test case of a 2D barge in waves

3 Results for a 2D Barge in Waves

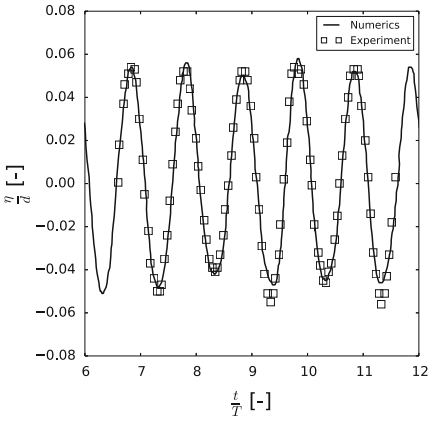
The capability of the presented 6DOF algorithm is presented for a rigid floating barge in two dimensions under the effect of waves with and without mooring. The results are compared to the experimental data of Ren et al. [19]. The laboratory experiment was performed in a wave flume of 20 m length, 0.8 m height and 0.44 m width, which is modelled with the numerical wave tank of REEF3D [4]. The barge is 0.30 m long and 0.2 m high. Since the gap between body and flume walls is small, the case can be considered as 2D, with surge, heave and pitch motion. The initial position of the barge is defined by its centroid at $(x, z) = (7.0 \text{ m}, 0.4 \text{ m})$ (see Fig. 2). Its density is 500 kg/m^3 . The water depth in the tank is $d = 0.4 \text{ m}$. The incoming waves are regular and have a height of 0.04 m, a period of $T = 1.2 \text{ s}$ and wavelength of 1.936 m. In the calculations, these are modelled using a second-order Stokes wave theory. A numerical beach is applied in order to avoid wave reflections at the outlet. For the discretisation, a cell size of 0.005 m is chosen which equals 640,000 cells.

3.1 Free-Floating Condition

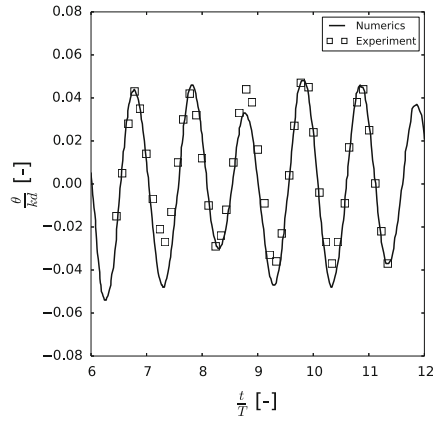
The results from the free-floating simulation are compared with the experiment for the period between $t/T = 6.36 \text{ s}$ and $t/T = 12 \text{ s}$. The wave elevation shown in Fig. 3a shows a good agreement with the experimental data, which confirms the chosen wave theory for modelling the waves. In accordance with the quality of the incoming waves, the distribution of the pitch motion predicts accurate results for the most part of the simulation. Small undershoots are given which correspond to underpredicted wave troughs at $t/T = 9.3$ and $t/T = 11.3$ (see Fig. 3b). Also, underresolved damping effects from vortex detaching at the immersed edges might influence the accuracy of the pitch motion. The frequency of the heave motion follows the frequency of the experimental data accurately. However, the amplitudes of this motion are 10% smaller in the simulations. This might be caused by the coupled physics of heave and pitch motion. In contrast, the surge motion is predicted much better, showing a good accordance of the drift with the experiments. This drift is mainly caused by inertia effects driven by the wave motion which is accurately predicted here (Fig. 3b).

3.2 Moored Condition

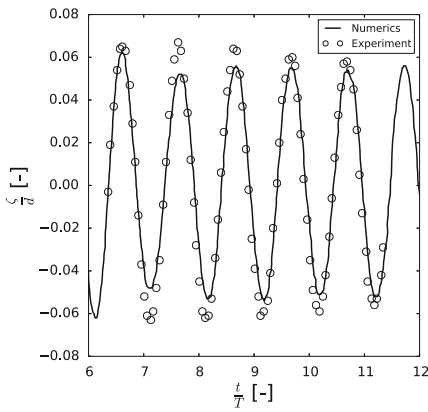
The effect of mooring and capability of the presented mooring model are shown for the 2D barge in waves. For this purpose, two mooring lines are fixed to the body at $z = 0.4 \text{ m}$ (Fig. 4). The cables are 1.6 m long, 0.01 m thick and have a weight per unit length of $w = 4 \text{ kg/m}$ in water. A comparison to the motion from above is ensured by increasing the weight of the free-floating body resulting in the same draft as the



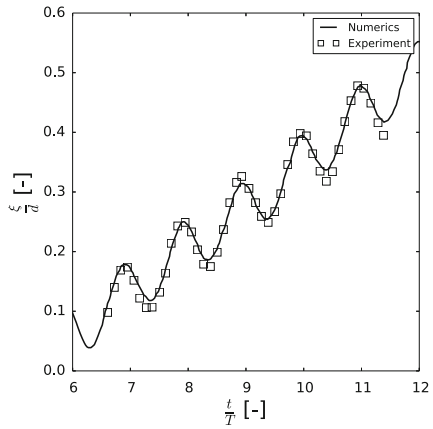
(a) Wave elevation at $x = 5.5$ m.



(b) Pitch motion.



(c) Heave motion.



(d) Surge motion.

Fig. 3 Numerical results of the two-dimensional barge in comparison to the experiment data

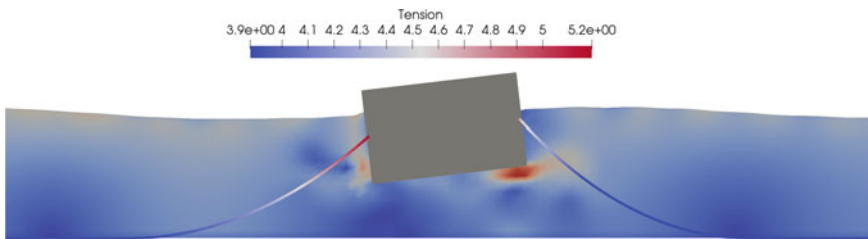


Fig. 4 Tension force distribution in the mooring cables during a wave trough situation

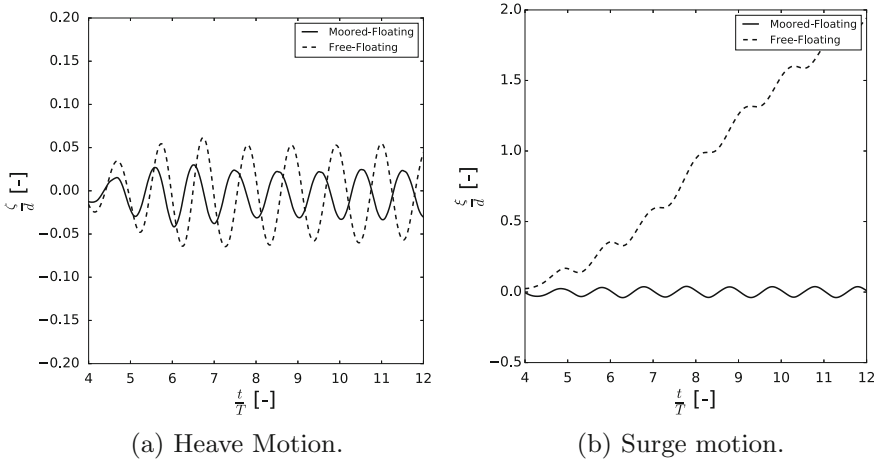


Fig. 5 Numerical results of the free-floating and moored-floating two-dimensional barge

initial condition. As result, the heave and surge motions over time are shown in Fig. 5. The vertical motion of the structure is significantly damped by installing the mooring system. Further, surging is prevented almost completely.

4 Conclusion

This paper gives an overview of the implementation of a weakly coupled 6DOF algorithm in the open-source CFD code REEF3D. The floating body is represented by the combination of a surface mesh, a level set function and the ghost cell immersed boundary method. This results in a method that does not require re-meshing or overset grids. In addition, a simple mooring model is presented which provides analytical solutions for the shape and forces of mooring systems. The application confirms the accuracy of REEF3D in modelling fluid–structure interactions. The mooring model is able to provide the damping effects on the motion of floating bodies. However, for more advanced mooring applications, like tension-leg platforms and extreme weather situations, a dynamic model is preferable.

Acknowledgements The calculations were supported in part with computational resources at the Norwegian University of Science and Technology (NTNU) provided by NOTUR project (No. NN2620K), <http://www.notur.no>.

References

1. Aamo OM, Fossen TI (2001) Finite element modelling of Moored vessels. *Math Comput Model Dyn Syst* 7(1):47–75
2. Berthelsen PA, Faltinsen OM (2008) A local directional ghost cell approach for incompressible viscous flow problems with irregular boundaries. *J Comput Phys* 227:4354–4397
3. Bihs H, Kamath A (2017) A combined level set/ghost cell immersed boundary representation for floating body simulations. *Int J Numer Meth Fluids* 83:905–916
4. Bihs H, Kamath A, Alagan-Chella M, Aggarwal A, Arntsen ØA (2016) A new level set numerical wave tank with improved density interpolation for complex wave hydrodynamics. *Comput Fluids* 140:191–208
5. Brackbill JU, Kothe DB, Zemach C (1992) A continuum method for modeling surface tension. *J Comput Phys* 100(2):335–354
6. Calderer A, Kang S, Sotiropoulos F (2014) Level set immersed boundary method for coupled simulation of air/water interaction with complex floating structures. *J Comput Phys* 277:201–227
7. Carrica PM, Noack RW, Stern F (2007) Ship motions using single-phase level set with dynamic overset grid. *Comput Fluids* 36:1415–1433
8. Chorin A (1968) Numerical solution of the Navier-Stokes equations. *Math Comput* 22:745–762
9. Davidson J, Ringwood J (2017) Mathematical modelling of mooring systems for wave energy converters—a review. *Energies* 10:666
10. Faltinsen OM (1990) *Sea loads on ships and offshore structures*. Cambridge University Press, Cambridge
11. Fossen TI (1994) *Guidance and control of ocean vehicles*. Wiley, Chichester, England
12. Hall M, Goupee A (2015) Validation of a lumped-mass mooring line model with DeepCwind semisubmersible model test data. *Ocean Eng* 104:590–603
13. Huang S (1994) Dynamic analysis of three-dimensional marine cables. *Ocean Eng* 21:587–605
14. Jiang GS, Peng D (2000) Weighted ENO schemes for Hamilton Jacobi equations. *SIAM J Sci Comput* 21:2126–2143
15. Jiang GS, Shu CW (1996) Efficient implementation of weighted ENO schemes. *J Comput Phys* 126(1):202–228
16. Osher S, Sethian JA (1988) Fronts propagating with curvature-dependent speed: algorithms based on Hamilton-Jacobi formulations. *J Comput Phys* 79:12–49
17. Peng D, Merriman B, Osher S, Zhao H, Kang M (1999) A PDE-based fast local level set method. *J Comput Phys* 155:410–438
18. Ramaswamy B, Kawahara M, Nakayama T (1986) Lagrangian finite element method for the analysis of two-dimensional sloshing problems. *Int J Numer Methods Fluids* 6:659–670
19. Ren B, He M, Dong P, Wen H (2015) Nonlinear simulations of wave-induced motions of a freely floating body using WCSPPH method. *Appl Ocean Res* 50:1–12
20. Shu CW, Osher S (1988) Efficient implementation of essentially non-oscillatory shock-capturing schemes. *J Comput Phys* 77(2):439–471
21. Sussman M, Smereka P, Osher S (1994) A level set approach for computing solutions to incompressible two-phase flow. *J Comput Phys* 114:146–159
22. Udaykumar HS, Mittal R, Rampungoon P, Khanna A (2001) A sharp interface cartesian grid method for simulating flows with complex moving boundaries. *J Comput Phys* 174:345–380
23. van der Vorst H (1992) BiCGstab: a fast and smoothly converging variant of Bi-CG for the solution of nonsymmetric linear systems. *SIAM J Sci Comput* 13:631–644
24. Yang J, Balaras E (2006) An embedded-boundary formulation for large-Eddy simulation of turbulent flows interacting with moving boundaries. *J Comput Phys* 215:12–40
25. Yang J, Stern F (2014) Robust and efficient setup procedure for complex triangulations in immersed boundary simulations. *J Fluids Eng* 135(10):101107.1101107.11
26. Yang J, Stern F (2012) A simple and efficient direct forcing immersed boundary framework for fluidstructure interactions. *J Comput Phys* 231:5029–5061
27. Zhang J, Jackson TL (2009) A high-order incompressible flow solver with WENO. *J Comput Phys* 228:146–159